Korean J. Chem. Eng., **30**(3), 658-663 (2013)
DOI: 10.1007/s11814-012-0167-0

Adsorption backup following light-emitting diode-irradiated photocatalytic unit for control of low-degraded toxic gaseous compounds

Wan-Kuen Jo†

Department of Environmental Engineering, Kyungpook National University, Daegu 702-701, Korea
(*Received 24 June 2012 • accepted 30 September 2012*)

Abstract−Although several visible light-emitting diode (LED)-irradiated photocatalysts exhibited low photocatalytic decomposition efficiencies for toxic gaseous pollutants, activated carbon fiber (ACF) has rarely been used as a backup adsorption device for photocatalytic systems. Accordingly, this study accessed the applicability of a supplemental ACF following a visible LED-irradiated S-TiO_2 unit for the control of low-degraded benzene and toluene. The characteristics of the S-TiO_2 and ACF were determined using an XRD, a UV-Vis-NIR, and an FTIR spectrophotometer. For an LED/S-TiO_2 system, low degradation efficiencies regarding benzene and toluene (close to zero-7.2% and 7.1-64.4%, respectively) were found. In contrast, the mean degradation efficiencies of both compounds obtained from the photocatalytic-ACF hybrid system were all close to 100%. In addition, no peaks were observed in the gas chromatogram of air samples taken at the outlet of the hybrid system, whereas several trace peaks were observed in the stand-alone photocatalytic reactor results. The breakthrough of the ACF occurred at approximately 14 and 28 hours for benzene and toluene, respectively, and saturation occurred at approximately 28 and 42 hours, respectively. Consequently, this study newly found that the supplemental activated carbon fiber following a visible LED-irradiated S-TiO_2 unit could be applied effectively for the control of low-degraded toxic benzene and toluene.

Key words: Supplemental Device, LED-irradiated S-doped TiO_2, Toxic Gas, Adsorption Capacity

INTRODUCTION

Heterogeneous photocatalysis has recently been found to be an attractive technique regarding the remediation of environmental pollutants [1-3]. This technology has the potential to degrade a broad range of volatile organic compounds (VOCs) to CO_2 and H_2O as a result of reactions either with molecular oxygen or with hydroxyl radicals and super-oxide ions formed after the initial production of highly reactive electron-hole pairs when photocatalysts are UV or visible-light irradiated [4,5]. The photocatalytic process over photocatalysts requires a light source that exceeds the band-gap energy of the photocatalysts. Recent studies [6-9] have suggested the use of light-emitting diodes (LEDs) as promising alternative light sources over conventional lamps for the photocatalytic processing of environmental pollutants. LEDs have several advantages over conventional light sources [10]. They are more efficient in converting electricity into light due to their close to unity high quantum yields, thereby leading to low electrical consumption. LEDs also have a long life and provide a tunable and nearly monochromatic light. Moreover, certain studies [7,9] have reported that LEDs could be energy-efficiently utilized as alternative light sources for the photocatalytic degradation of volatile dimethyl sulfide and formaldehyde under various operational conditions. Nevertheless, these studies emphasized that the LED/photocatalytic systems evidenced lower photocatalytic degradation efficiencies compared to conventional lamp/photocatalytic systems. This finding suggests that the application of an LED/photocatalytic system alone may not be sufficient to effectively control certain toxic VOCs that require high removal efficiency in order to minimize health risks from environmental exposure. In regards to such cases, the use of a supplemental device, such as an adsorption system, would aid in the further removal of toxic VOCs exiting from LED/photocatalytic systems without being decomposed.

The adsorption of VOCs by means of an activated carbon (AC) bed is a well-known technology with an effective removal efficiency, even at indoor concentration levels [11]. AC fibers (ACFs) are a newly developed type of photocatalyst support material consisting of nanographites. Compared to granular AC, ACF has a larger specific surface area, a superior rate of adsorption and desorption, and a faster attainment of adsorption equilibrium [12,13]. Nevertheless, ACF has rarely been used as a backup adsorption device for photocatalytic systems. Accordingly, the present study investigated the feasibility of the use of supplemental ACF materials following a visible LED-irradiated S-doped TiO_2 (S-TiO_2) unit to control low-degraded gaseous toxic compounds. Several studies have reported that S-TiO_2 exhibited a relatively high photocatalytic activity for environmental pollutants under visible-light irradiation [14-16], although these studies utilized conventional lamps for their visible-light source, such as a fluorescent daylight lamp or a mercury-xenon lamp. The target compounds, benzene and toluene, are frequently detected at high concentration levels in indoor as well as outdoor environments [17]; they are toxic or potentially toxic to humans [18].

EXPERIMENTAL

1. Experimental Set-up

The schematic diagram of the experimental set-up is presented in Fig. 1. The photocatalytic reactor and the ACF unit were con-

†To whom correspondence should be addressed.
E-mail: wkjo@knu.ac.kr

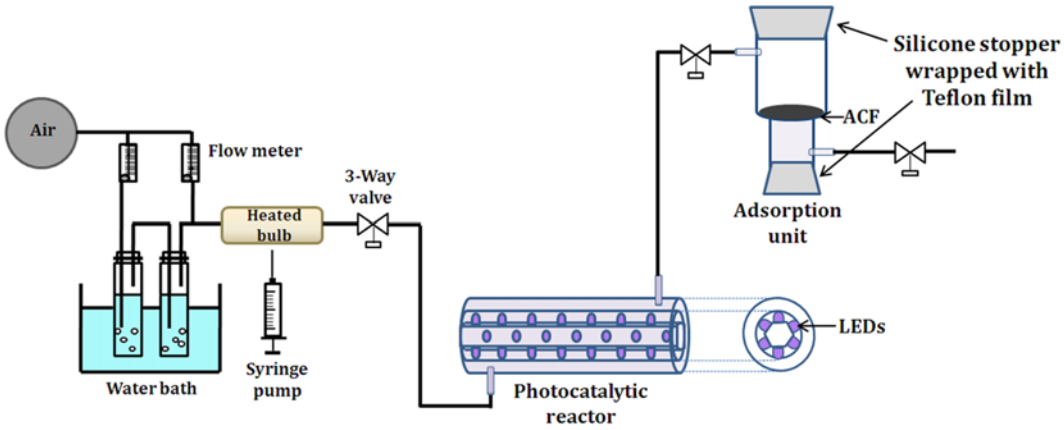

Fig. 1. Schematic diagram of experimental set-up.

nected in a tandem arrangement. The photocatalytic reactor had an annular geometry, and consisted of a glass tube coated on its inner surface with a thin film of an S-TiO_2 photocatalyst. A hexahedral tube with violet or blue LED bulbous lamps was inserted inside another Pyrex tube, whose outer surface served as the inner surface of the annular reactor. The hexahedral tube was made of Teflon (11×11×285 mm), as a support for the visible-light LEDs. The S-TiO_2 photocatalyst was prepared using the method employed by Ohno et al. (2004). In brief, titanium isopropoxide was mixed with thiourea, dried for 3 d, and then calcined at 500 °C. The prepared S-TiO_2 powder was coated on the inner surface of the reactors using the method employed by Xagas et al. [19]. In addition, viscose rayon-based ACF (Korean Activated Carbon Fiber) in the form of felt was purchased and washed with ultra-pure water and then, dried at 105 °C for 3 h prior to use. The carbon content, the surface area, and the micropore diameter of the ACF were 70 g m^{-2}, 1,000 m^2 g^{-1}, and 20 Å, respectively. A double-cylindrical Pyrex tube was utilized in order to contain the ACF (0.1 cm thickness and 6.2-cm diameter). Both the prepared S-TiO_2 powder and the ACF were characterized using an X-ray diffraction (XRD) meter (D/max-2500 diffractometer, Rigaku Inc.), a diffuse reflectance ultraviolet-visible-near infrared (UV-VIS-NIR) spectrophotometer (Model CARY 5G, Varian Inc.), and a Fourier transform infrared (FTIR) spectrophotometer (Spectrum GX, PerkinElmer Inc.).

Dried air was supplied by a zero-grade air cylinder. The humidity level was adjusted by passing the dried air through a charcoal filter, followed by a humidifying device in a water bath (HAAKE W26, Cole-Parmer Inc.). The relative humidity (RH) was measured, immediately prior to the photocatalytic reactor inlet, by using a humidity meter (Thermo Recorder TR-72S, T & D Co). The standard gas, which was prepared by injecting standard compounds into a mixing chamber via a syringe pump (model 210, KdScientific Inc.), flowed through the annular region of the photocatalytic reactor and then to the ACF unit. The stream flow rate (SFR) was controlled using rotameters calibrated against a dry gas meter.

2. Survey Design

This study included two different experiments: the comparison of the removal efficiencies as determined via a stand-alone photocatalytic reactor and a photocatalytic-ACF hybrid system and ACF breakthrough and saturation tests. Both experiments were performed under the following conditions: SFR, 1.0 L min^{-1}; input concentration (IC), 1.0 ppm (2.5 ppm for the latter experiment); and RH, 50%. For the former experiment, the light source was blue- or violet-LEDs. In addition, three operational parameters (SFR, RH, and IC) were evaluated for the removal efficiencies for benzene and toluene using the stand-alone photocatalytic reactor and the photocatalytic-ACF hybrid system. The SFRs were varied from 0.5 to 2.0 L min^{-1}. The RHs ranged from 10 to 90%. The test ICs involved 1, 3, 5, and 10 ppm. The target compounds were introduced after confirming that no contamination with the target compounds was measured in the system. A series of concentration measurements with respect to the target compounds were conducted at both the inlet and outlet of the photocatalytic reactor, ACF unit, or hybrid system. For the first experiment, six 10-min samples were collected over 3 h at 1 h intervals at the inlet and outlet openings. Since the series concentrations were similar, their average values were utilized in order to calculate the removal efficiency for the photocatalytic reactor, the ACF unit, and the hybrid system. For the second experiment, air samples were periodically collected for 48 h at the inlet and outlet of the ACF unit.

3. Sampling and Analysis

Gas samples were collected by filling an evacuated 5 L Tedlar bag at a constant flow rate. Air was then drawn through a sorbent trap containing 0.2 g of Tenax TA and 0.1 g of carboxen 569, using a constant flow-sampling pump (Aircheck Sampler Model 224-PCXR8, SKC Inc.). All of the samples were collected at ambient room temperatures (19-25 °C); the sampling flow rates were recorded at between 0.1 and 1 *l* min^{-1}. The target compounds collected on the sorbent trap were analyzed by coupling a thermal desorption system (Tekmar Model Aerotrap 6000) to a gas chromatograph (GC, Hewlett Packard 7890) in conjunction with a flame ionization detector (HP 5890II) or a mass spectrometer (HP MSD5973) (GC/MS) system using a 0.32-mm-id by 60-m-length fused silica column (Supelco Co. SPB-5).

The quality assurance/quality control program for the measurement of the gas-phase target compounds included laboratory blank traps and spiked samples. At the beginning of a test, a laboratory blank trap was analyzed in order to monitor any trap contamination. An external standard was analyzed daily in order to monitor the quantitative response. When the daily quantitative response differed by more than ±10% from that predicted by the specified calibration equation, a new calibration equation was determined. The method

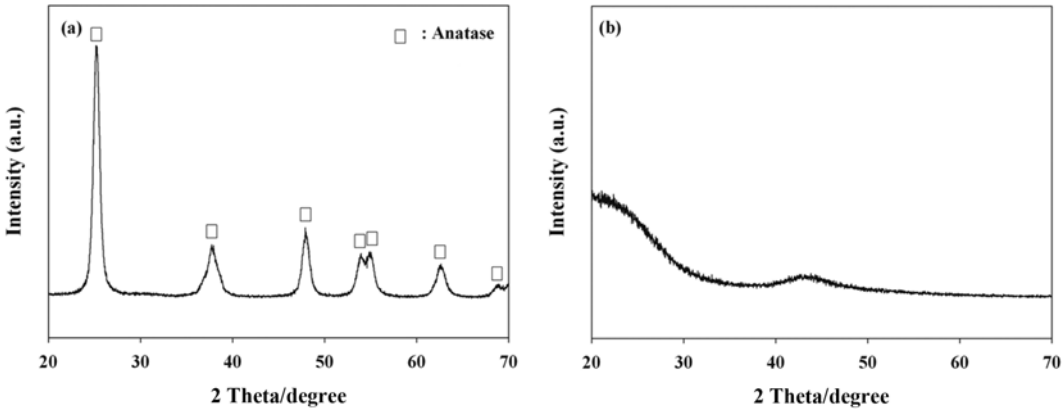

Fig. 2. X-ray diffraction spectra of S-doped TiO_2 and ACF.

detection limits ranged from 0.3 to 0.5 ppb for benzene and toluene, respectively.

RESULTS AND DISCUSSION

1. Characteristics of S-doped TiO_2 and ACF

Fig. 2 illustrates the XRD patterns of both the S-TiO_2 and ACF. The X-ray diffractogram of the S-TiO_2 powder exhibited well-defined diffraction peaks corresponding to the anatase crystal TiO_2 phase with a distinct peak at 2θ=25.3°, but without the distinctive peaks found for the rutile crystal TiO_2 phase. This result is consistent with that found for S-TiO_2 prepared at calcination temperatures lower than 600 °C by other researchers [14,15,20]. In contrast, Znad and Kawase [21] observed a few small peaks assigned to the rutile crystal TiO_2 phase for the S-TiO_2, which was synthesized using commercially-available Degussa P-25 TiO_2 and thiourea. In addition, the small peak located for the ACF at approximately 2θ=43° was assigned to graphite [22], which is reflective of the presence of carbon on the viscose rayon support regarding the ACG employed in the current study.

The UV-visible absorbance spectrum of the S-TiO_2 photocatalyst is presented in Fig. 3. A shift of the absorbance spectrum towards the visible light region was observed for the S-doped TiO_2 powders, whereas, according to previous studies [21,23], pure TiO_2 photocatalysts evidenced their absorption edge at λ=400-450 nm. This result agrees well with those reported by other studies [14,21,23]. The absorption edge for the S-doped TiO_2 was shifted to a λ>720 nm, which was attributable to the band gap narrowing of the TiO_2 by sulfur doping [14,24]. Consequently, it was indicated that the as-prepared S-doped TiO_2 powders could be effectively activated by visible-light irradiation.

Fig. 4 exhibits the FTIR spectra of the as-prepared S-doped TiO_2 powders. Major peaks were located at 3,411, 1,630, 1,151, and 604 cm^{-1}. Other researchers [25,26] have also reported main absorption peaks at similar frequencies for their S-doped TiO_2 samples. The band at 3,411 cm^{-1} was assigned to the O-H stretching vibration, whereas the band at 1,630 cm^{-1} was assigned to the O-H bending of the water molecules absorbed on the catalyst surface [25,26]. A peak at 1,151 cm^{-1} was ascribed to the stretching frequencies of the S-O bonds of sulfate ions [27], which would be produced by the dissociation of the thiourea. The correspondence of the band at 604 cm^{-1} was attributable to titanium crystal lattice vibrations [25].

2. Removal Efficiencies via Photocatalytic Reactor and Hybrid System

Fig. 5 shows the removal efficiencies of the benzene and toluene as determined over a 3-h period via the photocatalytic reactors

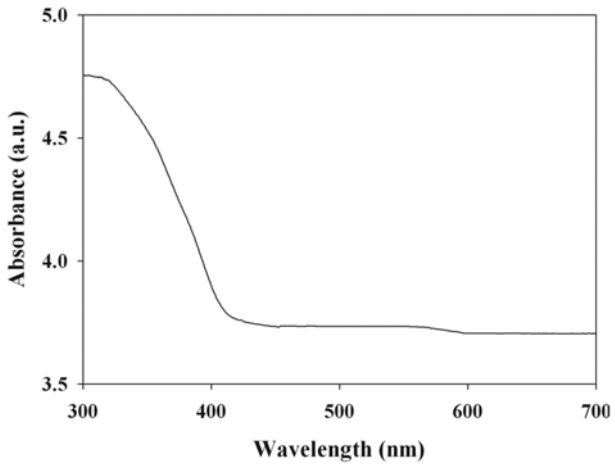

Fig. 3. Ultraviolet-visible spectrum of S-doped TiO_2.

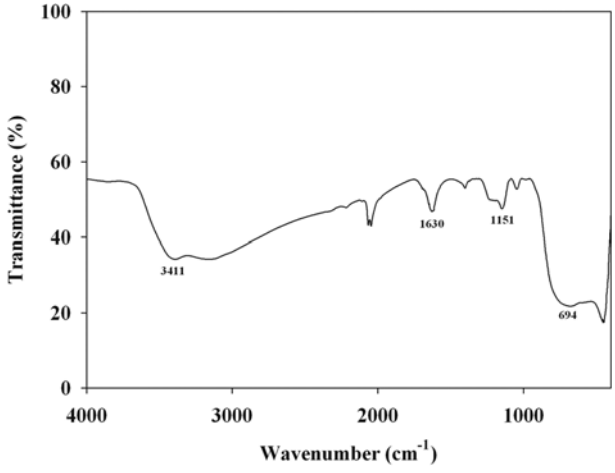

Fig. 4. Fourier transform infrared spectrum of S-doped TiO_2.

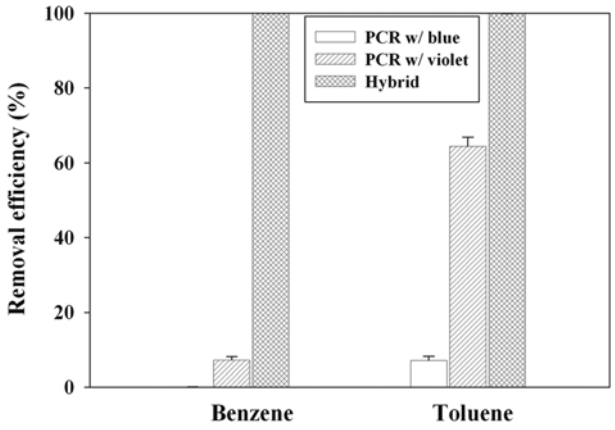

Fig. 5. Removal efficiencies (%)±standard deviation of benzene (IC, 1.0 ppm) and toluene (IC, 1.0 ppm) as determined over a 3-h period via photocatalytic reactor (PCR) with blue or violet LEDs and photocatalytic-ACF hybrid system.

using blue or violet LEDs and a photocatalytic-ACF hybrid system. The mean degradation efficiencies of the benzene and toluene obtained from the photocatalytic reactor using violet LEDs were 7.2 and 64.4%, respectively, whereas the mean degradation efficiencies obtained from the photocatalytic reactor using blue LEDs were close to zero and 7.1%, respectively. As indicated earlier, other studies [7,9] have also reported lower photocatalytic degradation efficiencies of gas-phase dimethyl sulfide and formaldehyde when LED/photocatalytic systems were applied. Benzene is a known carcinogen, inducing diseases such as leukemia [28], and toluene is a toxic chemical causing damage to the nervous system and liver [29]. The mean concentrations of benzene and toluene measured at the outlet of the photocatalytic reactor using blue LEDs were close to 1 ppm and 0.93 ppm, respectively. Even for the photocatalytic reactor using violet LEDs, the mean outlet concentrations of benzene (0.93 ppm) and toluene (0.36 ppm) exceeded the USEPA reference concentration (Rfc) of 30 μg m^3 (corresponding to 0.01 ppm) and 400 μg m^3 (corresponding to 0.11 ppm) with respect to benzene and toluene [30]. Therefore, the low degradation efficiencies of the two toxic compounds for the LED/photocatalytic system rationalize the application of the ACF, as a backup device to effectively control these compounds.

Fig. 5 also exhibits the degradation efficiencies of the benzene and toluene obtained from the photocatalytic-ACF hybrid system. Unlike the photocatalytic reactor alone, the mean degradation efficiencies of both compounds obtained from the photocatalytic-ACF hybrid system were all close to 100%. Previous studies [31,32] have reported that specific byproducts can be generated during the photocatalytic processes regarding gaseous pollutants. In fact, although they were unidentified, several trace peaks were observed when the photocatalytic reactor alone was applied, suggesting the presence of byproducts in the gas samples. However, no peaks at all in the gas chromatogram were observed at the outlet of the photocatalytic-ACF hybrid system. This suggests that the supplemental ACF also removed the gas-phase byproducts which were generated during the photocatalytic process. Consequently, it was confirmed that the supplemental ACF following a visible LED-irradiated S-TiO_2 unit could be applied effectively for the control of low-degraded toxic benzene and toluene.

Table 1. Comparison of removal efficiencies (%) for benzene (IC, 1.0 ppm) and toluene (IC, 1.0 ppm) determined via photocatalytic reactors with violet LEDs and photocatalytic-ACF hybrid system under different relative humidity (%) conditions

Compounds	System	Relative humidity			
		10	50	70	90
Benzene	Photocatalytic reactor	12.6	8.3	8.5	5.4
	Hybrid system	~100	~100	~100	88.7
Toluene	Photocatalytic reactor	81.3	63.4	62.7	48.5
	Hybrid system	~100	~100	~100	93.2

The humidity effect on the removal efficiency was investigated using four RHs (10, 50, 70, and 90%) that cover dry and humid environments. Table 1 shows the removal efficiencies for benzene and toluene concentrations determined using the photocatalytic reactors with violet LEDs and the photocatalytic-ACF hybrid system under different RH conditions. For the photocatalytic reactors, the removal efficiencies exhibited a general decreasing pattern with the RH increases. This pattern is attributable to the result of competitive adsorption between water and the contaminant on the catalyst surface [33]. This result confirms that water vapors are an important parameter for photocatalytic oxidation processes of the S-TiO_2 photocatalyst prepared in the present study. For the hybrid system, however, the removal efficiencies were close to 100% for both benzene and toluene. Consequently, it was suggested that the application of a hybrid system rather than stand-alone photocatalytic system is strongly recommended to remove effectively benzene and toluene under high humidity environments.

Table 2 exhibits the effect of SFR, which is related to residence time and face velocity in reactors, on the removal efficiencies for benzene and toluene. For the photocatalytic unit, the removal decreased as the SFR was increased. For two highest SFRs (1.5 and 2.0 L min^{-1}), the removal efficiencies determined using this unit were <1% for both benzene and toluene. This pattern is ascribed to an insufficient reactor residence time or mass transfer due to high flow rate [34]. The residence times, which were calculated by dividing the reactor volume by flow rate, were 26.4, 13.2, 8.8, and 6.6 s for the flow rates of 0.5, 1.0, 1.5, and 2.0 L $minute^{-1}$, respectively. In contrast, the removal efficiencies determined using the hybrid system were close to 100% for both benzene and toluene, thereby implying the application of a hybrid system rather than a photocat-

Table 2. Comparison of mean removal efficiencies (%) for benzene and toluene determined via photocatalytic reactors with violet LEDs and photocatalytic-ACF hybrid system under different flow-rate (L min^{-1}) conditions

Compounds	System	Flow rate			
		0.5	1.0	1.5	2.0
Benzene	Photocatalytic reactor	15.4	8.3	<1	<1
	Hybrid system	~100	~100	~100	~100
Toluene	Photocatalytic reactor	77.3	63.4	<1	<1
	Hybrid system	~100	~100	~100	~100

Table 3. Comparison of removal efficiencies (%) for benzene and toluene determined via photocatalytic reactors with violet LEDs and photocatalytic-ACF hybrid system under different input concentration (ppm) conditions

Compounds	System	Input concentration			
		1	3	5	10
Benzene	Photocatalytic reactor	8.3	5.2	<1	<1
	Hybrid system	~100	~100	81.2	67.8
Toluene	Photocatalytic reactor	63.4	51.7	34.2	15.5
	Hybrid system	~100	~100	91.4	84.2

alytic unit when high flow rates are required.

Table 3 shows the benzene and toluene removal efficiencies as determined using the photocatalytic system and the hybrid system according to the ICs. In most cases, removal efficiencies obtained from the photocatalytic system revealed a decreasing trend with increasing ICs. This result is consistent with those of other studies [35,36]. This removal efficiency dependence on ICs is ascribed to a competition of pollutant molecules for adsorption sites on the S-TiO_2 photocatalyst surface, because the adsorption of pollutants is an important factor for photocatalytic degradation efficiencies [37]. The competitive adsorption rate would be even greater at higher IC levels. In contrast, the removal efficiencies for both benzene and toluene as determined using the hybrid system were much higher than those determined using the photocatalytic unit alone. This indicates that the hybrid system can be applied more effectively to control high-level benzene and toluene compared to the photocatalytic unit alone.

3. Breakthrough and Saturation Property of ACF

To further understand the breakthrough and saturation properties of the ACF unit, the benzene and toluene concentrations were measured at the inlet and outlet of the ACF unit, without connecting any photocatalytic reactor upstream. Fig. 6 represents the breakthrough and saturation curves of the benzene and toluene as determined using the ACF unit. A roll-up effect for benzene was observed after being saturated, suggesting that water molecules displace the benzene molecules adsorbed earlier on the surface of the ACF. Similarly, Águeda

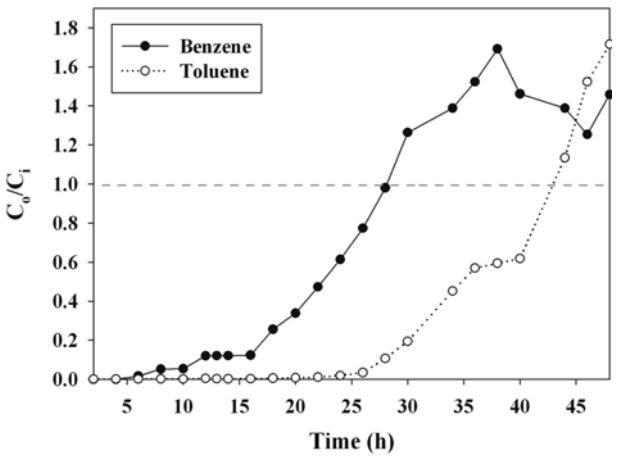

Fig. 6. Breakthrough and saturation curves of benzene (IC, 2.5 ppm) and toluene (IC, 2.5 ppm) as determined using the ACF unit.

Table 4. Adsorption capacity (mg g^{-1}), breakthrough time (h), saturation period (h) of the ACF, and initial concentrations (mg m^{-3}) for benzene and toluene

Compound	Adsorption capacity	Breakthrough time	Saturation period	Initial concentration
Benzene	32	14	28	7.5
Toluene	44	28	42	9.0

et al. [38] observed a similar roll-up effect when activated carbon monoliths were applied for the removal of gas-phase dichloromethane. According to the outlet to inlet concentration ratios, the breakthrough occurred at approximately 14 and 28 h for benzene and toluene, respectively; the saturation occurred at approximately 28 and 42 h, respectively, as given in Table 4. Similarly to this study, Sidheswaran et al. [13] found that toluene exhibited a longer breakthrough and saturation time compared to benzene. The longer breakthrough and saturation times for toluene are ascribed to a decrease in solubility and an increase in molecular weight [39]. The decrease in its solubility reflects the decrease in affinity with the water molecules on the AC surface, thereby resulting in less adsorption [40]. In contrast, Sidheswaran et al. [13] and Yao et al. [41] reported the saturation time of toluene or other VOCs on certain ACFs to be 197 and 97 h, respectively. This difference in saturation time is ascribed to the difference in experimental conditions, such as the properties and amounts of ACF employed, the initial concentrations of the target compounds, and the gas flow rates.

The adsorption capacity of the ACF used in this study was estimated using the inlet and outlet concentrations obtained during the adsorption processes, and the following equations:

$$A_c = M_t / M_f \quad (1)$$

$$M_t = \sum_{j=1}^{j-1} m_j \quad (2)$$

$$m_j = \int_0^t (C_{in} - C_{out,j}(t)) Q dt \quad (3)$$

where A_c is the adsorption capacity of benzene or toluene on the ACF (mg g^{-1}); M_f is the mass of the ACF (g); M_t is the total mass of benzene or toluene adsorbed on the ACF (mg); m_j is the mass of benzene or toluene adsorbed on the ACF (mg) during the jth adsorption period; C_{in} is the inlet concentration of benzene or toluene (mg m^{-3}); $C_{out,j}(t)$ is the outlet concentration of benzene or toluene (mg m^{-3}) obtained downstream of the ACF during the jth adsorption period; and Q is the adsorption flow rate (m^3 min^{-1}). Table 1 presents the adsorption capacity of the benzene and toluene on the ACF. The total benzene and toluene masses adsorbed on the ACF were 32 and 44 mg g^{-1}, respectively. The sum (76 mg) of the benzene and toluene masses adsorbed on 1 g of ACF was slightly lower than the toluene mass (81.6 mg) per gram of ACF reported by Yao et al. [41] and the VOC mixture mass (90.7 mg) per gram of ACF reported by Sidheswaran et al. [13]. Nevertheless, the difference in the adsorption capacities between this study and the Yao et al.'s study was less than 10%. In addition, according to both this study and the Sidheswaran et al. study, benzene, which was chosen in this study as a target compound, had a lower adsorption capacity relative to toluene or other aromatic VOCs. Accordingly, it is suggested that the

ACF employed in the present study was comparable to that of the previous studies with respect to the VOC adsorptions.

CONCLUSION

Although LEDs may be utilized as energy-efficient alternative light sources for the photocatalytic degradation of certain gaseous pollutants, their application to certain photocatalytic units may be limited due to their low photocatalytic degradation efficiencies, particularly for toxic gases. Therefore, this study investigated the applicability of a supplemental ACF following a visible LED-irradiated S-TiO_2 unit for the control of low-degraded benzene and toluene. The spectral investigations of an as-prepared S-TiO_2 photocatalyst and ACF supported their removal potentials for benzene and toluene. However, low degradation efficiencies of the two toxic compounds were obtained in the LED/S-TiO_2 system, thereby rationalizing the application of the ACF, as a backup device to effectively control benzene and toluene. Consequently, this study newly suggested that the supplemental activated carbon fiber following a visible LED-irradiated S-TiO_2 unit could be applied effectively for the control of low-degraded toxic benzene and toluene.

ACKNOWLEDGEMENTS

This work was supported by the National Research Foundation of Korea (NRF) grant funded by the Korea government (MEST) (No. 2011-0027916). I would like to thank two graduate students (In-Woo, Choi and Kun-Hwan Kim) in the Department of Environmental Engineering, Kyungpook National University, for their experimental set-up, sample collecting and/or analyses.

REFERENCES

1. Y. S. You, K.-H. Chung, Y. M. Kim, J.-H. Kim and G. Seo, *Korean J. Chem. Eng.*, **20**, 58 (2003).
2. L. Laokiat, P. Khemthong, N. Grisdanurak, P. Sreearunothai, W. Pattanasiriwisawa and W. Klysubun, *Korean J. Chem. Eng.*, **29**, 377 (2012).
3. A. Bernabeu, R. F. Vercher, L. Santos-Juanes, P. J. Simón, C. Lardín, M. A. Martínez, J. A. Vicente, R. González, C. Llosá, A. Arques and A. M. Amat, *Catal. Today*, **161**, 235 (2011).
4. T. Van Gerven, G. Mul, J. Moulijn and A. Stankiewicz, *Chem. Eng. Process.*, **46**, 781 (2007).
5. S. Malato, P. Fernández-Ibáñez, M. I. Maldonado, J. Blanco and W. Gernjak, *Catal. Today*, **147**, 1 (2009).
6. T. Matsumoto, N. Iyi, Y. Kaneko, K. Kitamura, S. Ishihara, Y. Takasu and Y. Murakami, *Catal. Today*, **120**, 226 (2007).
7. J. L. Shie, C. H. Lee, C. S. Chiou, C. T. Chang, C. C. Chang and C. Y. Chang, *J. Hazard. Mater.*, **155**, 164 (2008).
8. J. P. Ghosh, R. Sui, C. H. Langford, G. Achari and C. P. Berlinguette, *Water Res.*, **43**, 4499 (2009).
9. W. K. Jo, S. S. Eun and S. H. Shin, *Photochem. Photobiol.*, **87**, 1016 (2011).
10. Wikipedia, Light-emitting diode (2011). Accessed at http://en.wikipedia.org/wiki/Light-emitting_diode.
11. F. Haghighat, C.-S. Lee, B. Pant, G. Bolourani, N. Lakdawala and A. Bastani, *Atmos. Environ.*, **42**, 8176 (2008).
12. D. Das, V. Gaur and N. Verma, *Carbon*, **42**, 2949 (2004).
13. M. A. Sidheswaran, H. Destaillats, D. P. Sullivan, S. Cohn and W. J. Fisk, *Build. Environ.*, **4**7, 357 (2012).
14. T. Ohno, M. Akiyoshi, T. Umebayashi, K. Asaim, T. Mitsui and M. Matsumura, *Appl. Catal. A*, **265**, 115 (2004).
15. C. Han, M. Pelaez, V. Likodimos, A. G. Kontos, P. Falaras, K. O'Shea and D. D. Dionysiou, *Appl. Catal. B*, **107**, 77 (2011).
16. G. Yang, Z. Yan and T. Xiao, *Appl. Surf. Sci.*, **258**, 4016 (2012).
17. T. Ohura, T. Amagai, X. Shen, S. Li, P. Zhang and L. Zhu, *Atmos. Environ.*, **43**, 6352 (2009).
18. OEHHA (Office of Environmental Health Hazard Assessment), Proposition 65 Status Report Safe Harbor Levels: No Significant Risk Levels for Carcinogens and Maximum Allowable Dose Levels for Chemicals Causing Reproductive Toxicity, California Environmental Protection Agency, OEHHA, Sacramento, CA (2003). Accessed at http://www.oehha.ca.gov/prop65/pdf/june2003StatusReport.pdf.
19. A. P. Xagas, E. Androulaki, A. Hiskia and P. Falaras, *Thin Solid Films*, **357**, 173 (1999).
20. L. Szatmáry, S. Bakardjieva, J. Šubrt, P. Bezdička, J. Jirkovský, Z. Bastl, V. Brezová and M. Korenko, *Catal. Today*, **161**, 23 (2011).
21. H. Znadand and Y. Kawase, *J. Mol. Catal. A*, **314**, 55 (2009).
22. S. Yao, J. Li and Z. Shi, *Particuology*, **8**, 272 (2010).
23. E. M. Rockafellow, L. K. Stewart and W. S. Jenks, *Appl. Catal. B*, **91**, 554 (2009).
24. M. Ksibi, S. Rossignol, J.-M. Tatibouët and C. Trapalis, *Mater. Lett.*, **62**, 4204 (2008).
25. R. Bacsa, J. Kiwi, T. Ohno, P. Albers and V. Nadtochenko, *J. Phys. Chem. B*, **109**, 5994 (2005).
26. S. Liu and X. Chen, *J. Hazard. Mater.*, **152**, 48 (2008).
27. X. Wang, J. C. Yu, P. Liu, X. Wang, W. Su and X. Fu, *J. Photochem. Photobiol. A*, **179**, 339 (2006).
28. IARC (International Agency for Research on Cancer), *Monographs on the evaluation of the carcinogenic risks of chemicals to humans*, WHO, Geneva (2004).
29. A. S. Revilla, C. R. Pestana, G. L. Pardo-Andreu, A. C. Santos, S. A. Uyemura, M. E. Gonzales and C. Curti, *Toxicol. Vitro*, **21**, 782 (2007).
30. IRIS, IRIS database for risk assessment, US Environmental Protection Agency, (2005). Acessed at: http://www.epa.gov/iris/.
31. M. Mohseni, *Chemosphere*, **59**, 335 (2005).
32. X. Ye, D. Chen, J. Gossage and K. Li, *J. Photochem. Photobiol. A*, **183**, 35 (2006).
33. P. Pichat, *Appl. Catal. B*, **99**, 428 (2010).
34. T. Van Gerven, G. Mul, J. Moulijn and A. Stankiewicz, *Chem. Eng. Prog.*, **46**, 781 (2007).
35. A. Bouzaza, C. Vallet and A. Laplanche, *J. Photochem. Photobiol. A*, **177**, 212 (2006).
36. W. K. Jo and J. T. Kim, *J. Chem. Technol. Biotechnol.*, **85**, 485 (2009).
37. J. Zhao and X. Yang, *Build. Environ.*, **38**, 645 (2003).
38. V. Águeda, B. D. Crittenden, J. A. Delgado and S. R. Tennison, *Sep. Purif. Technol.*, **78**, 54 (2011).
39. A. A. M. Daifullah and B. S. Girgis, *Colloids Surf. A*, **214**, 181 (2003).
40. M. P. Cal, M. J. Rood and S. M. Larson, *Gas Sep. Purif.*, **10**, 117 (1996).
41. M. Yao, Q. Zhang, D. W. Hand, D. L. Perram and R. Taylor, *J. Air Waste Manage. Assoc.*, **59**, 31 (2009).